5-2012

Study of the Anisotropic Frictional and Deformation Behavior of Surfaces Textured with Silvr Nanorods

Thomas Ivanoff
University of Arkansas, Fayetteville

STUDY OF THE ANISOTROPIC FRICTIONAL AND DEFORMATION BEHAVIOR OF SURFACES TEXTURED WITH SILVER NANORODS

STUDY OF THE ANISOTROPIC FRICTIONAL AND DEFORMATION BEHAVIOR OF SURFACES TEXTURED WITH SILVER NANORODS

An Honors Thesis submitted in partial fulfillment of the requirements for Honors Studies in Mechanical Engineering and Physics

By

Thomas Alexander Ivanoff

2012

Mechanical Engineering
College of Engineering
&
Physics
J. William Fulbright College of Arts and Sciences
The University of Arkansas

This thesis is approved.

Thesis Advisor:

Dr. Min Zou

Thesis Committee:

Dr. Gay Stewart

Dr. John Stewart

Acknowledgements

The author would like to personally thank Dr. Min Zou for serving as the principle investigator on this study and providing a wealth of advice and support. The author would also like to thank Dr. Gay Stewart for her guidance in the making of this thesis.

Support provided from the University of Arkansas Honors College Undergraduate Research Grant, the Arkansas Biosciences Institute, and the US National Science Foundation under grants CMS-0645040 is gratefully acknowledged.

Support from Dr. Tansel Karabacak and Arif Sinan Alagoz at the University of Arkansas – Little Rock for developing and manufacturing the samples and technical advice is greatly appreciated.

Abstract

Friction is one of the most common and influential mechanical interactions of two structures on both the macroscopic scale and especially the microscopic scale. On the microscopic scale, friction becomes the prime component of mechanical forces exerted on devices. Frictional anisotropy is an interesting characteristic of certain materials and can be used to control frictional properties in various applications. In this study, we measured the anisotropic frictional behavior of two silver (Ag) thin films: a continuous film and a thin film consisting of tilted nanorods angled at an average angle of 70^{o} to the surface normal. Scratches, eight microns in length, were performed on the films with normal loads ranging from 50 μN to 8,000 μN using a conical tip with a 100 micron tip radius. The coefficient of friction (COF) of the tilted nanorods was measured for scratches performed along, against, and perpendicular to the tilt direction. In addition, the deformation of the individual scratches was visually characterized with a scanning electron microscope (SEM). The tilted nanorods demonstrated significant frictional anisotropy with the COF of scratches performed against the tilt direction being over 30 percent lower than those performed along the tilt direction. Furthermore, for normal loads up to 2000 μN, the tilted nanorod sample displayed a lower COF than the thin film for scratches performed against the tilt direction. Visual deformation analysis showed a large increase in damage as the normal load was systematically raised from 50 μN to 8000 μN. In addition, the deformations of the nanorods are shown to be dependent on the direction of the scratch.

Table of Contents

List of Figures

1. Introduction

1.1 Background

Friction is one of the most common and influential means by which two objects can mechanically interact. Everything from automobiles, to computers, to human joints encounter friction in various forms and strengths. Indeed, friction can be a useful force such as allowing the tires of a car to propel the vehicle forward and it can also be harmful to a process as in causing wear on human joints and electronic devices. Friction even controls the movement of massive objects such as glaciers (Zmitrowicz, 2003). Thus, because of its importance in nearly every discipline, friction has been studied for centuries.

Studies have focused on how to increase or eliminate friction or how to manipulate friction in a beneficial manner. One way to control the frictional behavior of a system is through surface topography modification (Ajayi, Erck, Lorenzo-Martin, & Fenske, 2009; Morton, Wang, Fleming, & Zou, 2011). Furthermore, surfaces can be modified in such a way that they exhibit friction anisotropy (Hirakata, Nishihira, Yonezu, & Minoshima, 2011; So, Demirel, & Wahl, 2010), different coefficients of friction in different directions.

Frictional anisotropy is a phenomenon that is observed naturally in certain crystalline structures when they slide along each other on different crystal planes (Enomoto & Tabor, 1980; Park et al., 2008). Animals and reptiles can also benefit from frictional

anisotropy. An example is the way in which snake abdomens are specially structured to exhibit friction anisotropy which greatly increases the snake's ability to move (Hao, Zhendong, & Songxiang, 2008). Another example is how the skin on a gecko's fingers is textured with microscopic tilted structures to allow it to climb walls and still be able to detach from the wall. Mimicking these phenomena in nature through surface texturing is one way that friction can be controlled in machine components (Hazel, Stone, Grace, & Tsukruk, 1999; Lee, Fearing, & Komvopoulos, 2008).

Nano-textured surfaces are vital to the improvement of the frictional properties of both micro-scaled and nano-scaled machines and electronic devices. The growing importance and application of micro-electro-mechanical-systems (MEMS) in everyday devices has made understanding friction behavior on the nano-scale essential to improve MEMS effectiveness and reliability. One of the challenges with producing efficient and long lasting MEMS is the need to take into account friction and adhesion forces that do not affect macroscopic objects, but do greatly affect micro-sized machines.

1.2 Adhesion Forces

Forces typically ignored in large objects are usually the most influential forces in the microscopic world. For example, there are several different types of adhesion mechanisms that can affect how two microscopic objects interact; some of the more common forms of adhesion forces present in MEMS devices include electrostatic, van der Waals, and capillary adhesion. When the surface spacing becomes less than 100 nm, each of the aforementioned adhesion forces becomes several orders of magnitude larger

than the typical restoring force of MEMS devices (Komvopoulos, 2003). Capillary adhesion can cause a liquid meniscus to form on the surface and retard motion. In addition, capillary adhesion forces are related to the relative humidity of the operating environment and therefore can vary greatly in strength. While capillary and electrostatic adhesion may not always exist, van der Waals attraction between the sample surface and the nanoindenter tip is always present. Indeed, it was not possible to distinguish if capillary, van der Waals, or electrostatic adhesion forces were solely responsible for affecting this study. In addition, there were no signs of chemical adhesion during this study, which was expected as the silver samples and diamond indenter tip do not undergo any chemical changes during contact with each other. However adhesion in some form was assumed to affect the friction testing. Thus discovering a way of reducing adhesion effects is necessary to improving the functionality of MEMS in real world applications. Surface texturing has the ability to reduce adhesion forces when compared to smooth thin films, due to larger separation and smaller contact area between contacting surfaces, and sometimes a lower surface energy created by the textured topography. It is becoming increasingly clear that the use of nano-textured surfaces is one of the most reasonable and effective ways to manipulate and control friction forces (Morton et al., 2011; Nair & Zou, 2008; Zou, Cai, Wang, Yang, & Wyrobek, 2005; Zou, Seale, & Wang, 2005; Zou et al., 2006; Zou, Cai, & Wang, 2006). In addition, the ability to vary friction coefficients in multiple directions allows for nano-textured surfaces to control the effects of the aforementioned adhesion forces in MEMS devices.

This study compares the frictional behavior of two silver thin films on glass substrates; one is a surface textured with angled nanorods while the other is simply a continuous thin film. The nano-textured surface was tested for anisotropic frictional behavior, in order to determine its potential for application in small devices as a means of directional manipulation of frictional forces. The textured surface displayed highly anisotropic frictional behavior. Furthermore, deformation analysis of the samples showed a striking contrast between the deformations of the two surfaces. Also, the nanorods were shown to be able to decrease contact area under low load conditions.

2. Experimental Details

2.1 Sample Preparation

Both the tilted nanorods sample and thin film sample were created using glancing angle deposition (GLAD) technique by Professor Tansel Karabacak's group at the University of Arkansas, Little Rock.

2.2 Equipment

The friction tests were conducted with a Hysitron nanoindenter – the TI 900 shown in Figure 1. The nanoindenter has the ability to sense both forces and displacements laterally as well as vertically through the use of a 3-plate capacitive system connected to the probing tip. Accordingly, the coefficient of friction (COF) is then determined from the lateral and vertical forces during the scratch.

Figure 1: Hysitron TI 900 Triboindenter.

An optical microscope is incorporated into the unit so that testing locations can be chosen on the sample surface. The direction of the scratch relative to the nanorod tilt direction could be adjusted by properly orienting the sample under the optical microscope. The scratch tests were conducted with a 90^{o} conical diamond tip with a 100 micron radius. A diagram of the forces and motions involved in a friction test are shown in Figure 2.

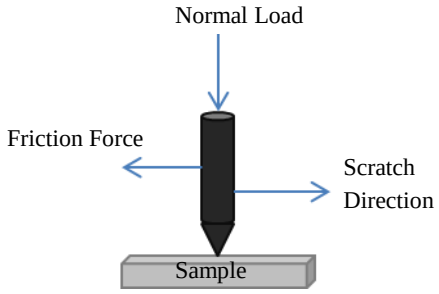

Figure 2: Diagram of friction tests.

After the scratch tests were completed on a particular sample, an environmental scanning electron microscope (ESEM, JEOL JSM-6335F) was used to visually characterize the deformation that the scratches caused to the thin film surfaces.

2.3 Procedure

The samples were prepared for testing in the nanoindenter by first securing them to a magnetic stainless steel disc with a small amount of high strength adhesive. A small cross-hair was manually scribed onto a clean corner of the thin film to allow for the scratches to be easily identified later on in the ESEM. In addition, the scribe was oriented on the nano-textured thin film in such a way that one line was perpendicular to the tilt

direction and the other was parallel to the tilt direction. The samples were then loaded into the nanoindenter and secured to the magnetic stage to ensure that they would remain stationary during testing.

The scratch tests consisted of a matrix of 55 individual scratches arranged into 11 vertical columns as shown in Figure 3. All of the scratches were 8 microns in length and the normal load was varied for each column and ranged from as low as 50 μN to as high 8000 μN; a detailed visualization of this test matrix is given by Morton (Morton et al., 2011). The 8 micron scratch length is the maximum scratch length of the equipment and was chosen to obtain the most data per scratch. Having five scratches in each column was to ensure that at least multiple scratches would be performed properly due to the inability to locate surface irregularities with the nanoindenter's optical microscope. The ESEM was able to identify any irregularities though, and verified that distorted and unanticipated COF data corresponded to irregular surface structures. However, both surfaces were observed to be very uniform and the multiple scratches became a means of confirming results through their repeatability.

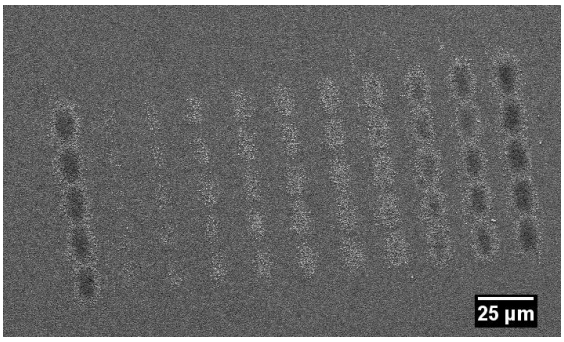

Figure 3: Full scratch matrix performed against the tilt direction.

The continuous thin film sample was tested twice. One test matrix was performed in an arbitrary direction because the thin film is uniform and the COF is the same in any scratching direction. The second matrix was performed in the counter scratching direction in regards to the first matrix to confirm the thin film's lack of friction anisotropy.

The tilted nanorod surface was more difficult to test than the continuous thin film sample. While the nanoindenter can move and sense forces in three directions, it is only capable of performing scratches along the Y-axis of its stage. Consequently, the position and orientation of the titled nanorod sample with respect to the stage was important to proper testing. Great care was taken to ensure that the manually scribed cross hair had one arm oriented parallel to the tilt direction and the other perpendicular to the tilt direction. The sample was then oriented appropriately on the nanoindenter stage for each test. A total of four scratch matrices were performed on this surface; one against the tilt direction, one along the tilt direction, and two perpendicular to the tilt direction. Figure 4 shows the four different scratching directions. The two perpendicular scratches were performed in the opposite direction of one another. Once the scratches along and against the tilt direction were performed, the sample was rotated 90^{o} to conduct the perpendicular tests.

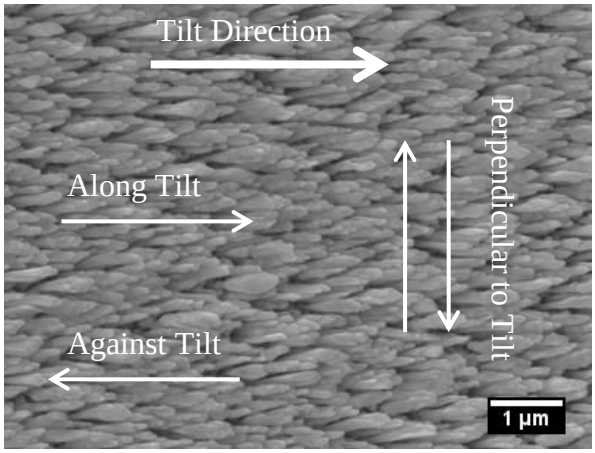

Figure 4: Diagram of the scratching directions.

After the scratch tests were performed an ESEM was used to visually characterize the deformation that each scratch caused to the surface. It was necessary to apply a light gold sputter to both of the samples to eliminate charging effects so that the individual nanorods could be observed. In addition, images were also obtained through the use of conductive tape without gold sputtering in order to determine what effect the sputter had on the surface topography. Indeed, the sputtering had a curious and advantageous affect that is discussed later. The manually scribed crosshair was used to help initially locate the scratched areas. Once within the vicinity of the scratched area, the different matrices were easily identifiable and scratches at each normal load were characterized for all of the scratching directions.

3. Results and Discussion

3.1 Surface Topography

Figure 5 shows the side and top down views of the nanorod sample. The side angle shows that the nanorods were grown at an average angle of 70^{o} to the surface normal. It can also be seen from the side view that smaller nanorod-like structures exist near the bases of the large nanorods. The size of the normal nanorods are fairly consistent, ranging from approximately 50 to 150 nanometers (nm) in diameter and are all about 1 micron in length. There is also very little clustering among the nanorods and a very linear arrangement to their positioning. The nanorods act as standalone structures for the majority of their length and are only in constant contact with each other near their bases. These characteristics allow for the tips of the nanorods to behave independently of each other. The nanorods are spaced on average 100 to 500 nm apart from each other at their bases.

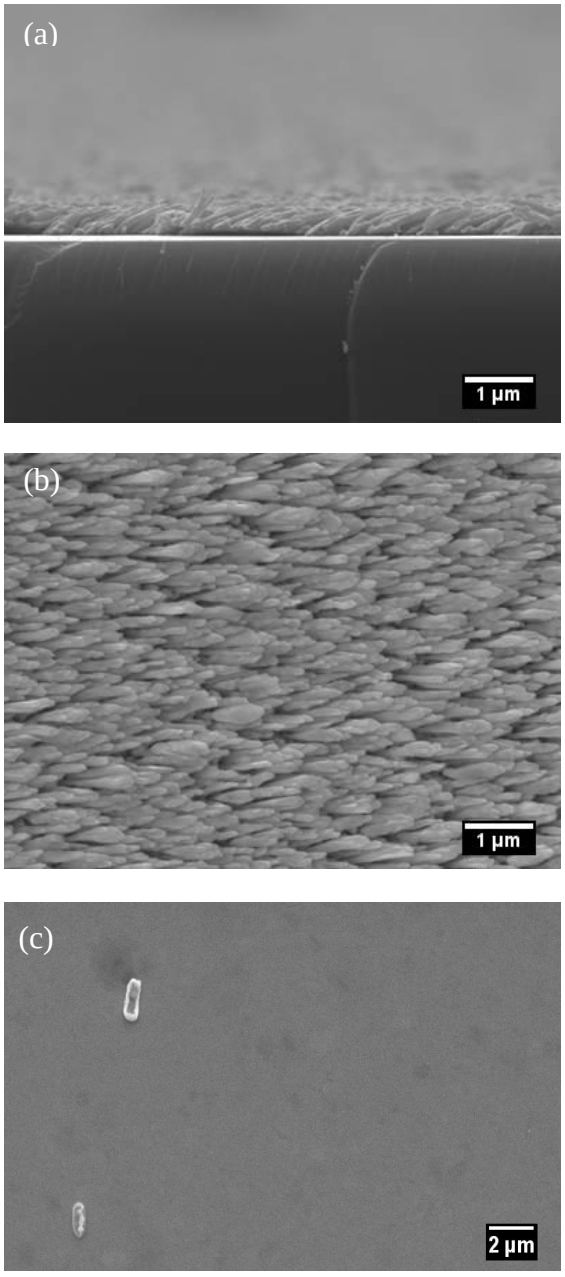

Figure 5: SEM crossectional view of (a) tilted nanorods. SEM top down view of (b) tilted nanorods and (c) thin film.

The nanorods were deposited on the surface in a continuous manner and created a film slightly less than half a micron thick. The thin film sample, as expected, is much

smoother and more consistent than the nanorod textured sample. There is very little variation in the surface topography as shown in Figure 5.

The tilted nanorod sample was created by using a glancing angle deposition (GLAD) technique. The GLAD technique is very versatile and can be used to create various patterns on the glass substrates with nanorod structures. The angle the nanorods form with respect to the surface normal can be altered as well.

3.2 Coefficient of Friction

The COF for both the thin film and all of the scratching directions of the nanorod textured sample are shown in Figure 6 and Table 1 up to scratches performed at normal loads of 2000 μN. For scratches of normal loads up to 250 μN, the thin film sample had the highest COF. Beyond 250 μN, the scratches performed both perpendicular and along the tilt direction on the nano-textured sample all have COF above those of the thin film. However, the COF for scratches performed against the tilt direction are the lowest of any direction. The COF for scratches done along the tilt direction are an average of 23 percent higher than those performed against the tilt.

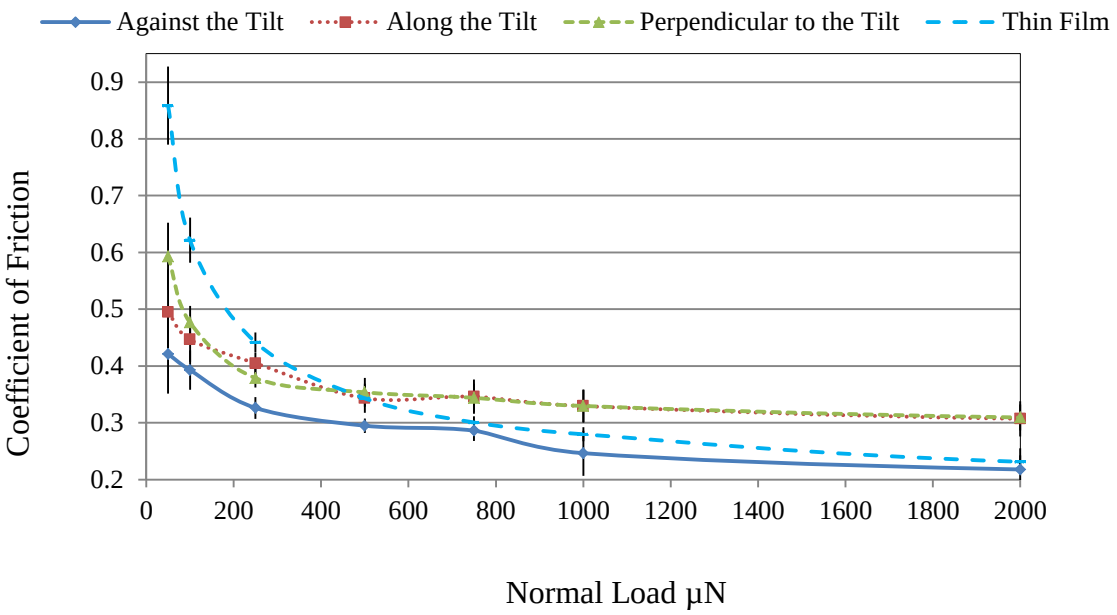

Figure 6: COF of the tilted nanorod sample and the thin film for scratching directions along, against, and perpendicular to the tilt direction.

This anisotropic behavior is in agreement with previous work performed where some samples displayed 20 percent anisotropic behavior (So et al., 2010). It must be noted that the scratches performed against the tilt direction do not ever yield a COF higher than the thin film.

Table 1: COF values.

Load (µN)	Against	Along	Perpendicular	Thin Film
50	0.421 ±0.070	0.495 ±0.075	0.593 ±0.059	0.859 ±0.069
100	0.393 ±0.035	0.447 ±0.040	0.477 ±0.029	0.621 ±0.040
250	0.326 ±0.019	0.405 ±0.020	0.379 ±0.017	0.442 ±0.017
500	0.295 ±0.013	0.343 ±0.025	0.354 ±0.026	0.343 ±0.010
750	0.286 ±0.018	0.346 ±0.030	0.344 ±0.025	0.301 ±0.011
1000	0.246 ±0.040	0.329 ±0.029	0.330 ±0.028	0.280 ±0.012
2000	0.218 ±0.037	0.307 ±0.031	0.309 ±0.023	0.231 ±0.011

In addition, the COF of scratches performed against the tilt direction gradually approach the level of that of scratches performed on the thin film. Scratches performed against the tilt were 49 percent, 86 percent, and 94 percent of the thin film at normal loads of 50 μN, 500 μN, and 2000 μN. The COFs of the scratches performed perpendicular to the tilt direction are nearly identical to those of the scratches performed along the tilt direction with the exception of loads 250 μN or less.

The COF for scratches performed against the tilt direction is lower than any other test on the nanorod textured surface due to the decrease in contact area during its scratching motion. As the nanoindenter's tip moves against the angle of the nanorods, it is prevented from digging into the film and rides along the top of the nanorods. When scratching along the nanorods' tilt direction, the tip also rides along the top of the nanorods but only at normal loads of less than 500 μN. Once the normal load is increased, the tip begins to bend the nanorods instead of riding along the top of them. This phenomenon is not experienced when running against the tilt direction until much higher loads, due to the fact that the nanorods are more easily bent toward the substrate than away from it. Thus, when the nanorods are bent and flattened, the tip sees a much higher contact area than before and this increases the COF. Furthermore, the tip is also able to penetrate deeper into the nanorods than the thin film when it scratches along the tilt direction due to the fact that the nanorods have gaps in between them and the thin film does not. This greater penetration causes the scratches performed along the tilt direction to have a higher COF

than the thin film at high normal loads. The tip does not dig into the sample while running against the tilt direction as much as when the tip is traveling along the tilt.

The scratches performed perpendicularly to the tilt behaved nearly identical to those performed along the tilt direction. This was a relatively unexpected result, as it was assumed that the perpendicular direction would yield a COF just under that of the along direction but still higher than scratches performed against the tilt. However, the fact that the perpendicular and along scratching directions are similar is not an unreasonable outcome. The nanorods were at first thought to be stronger and more resistant to bending horizontally, but in practice the nanorods proved to be too weak to resist the force of the nanoindenter. Likewise, the tip was able to become dug into the nanorods much like when traveling along the tilt direction, due to the nanorods not deflecting upward and forcing the indenter to travel along the tips of the nanorods. The COF for some of the individual scratches are displayed in Figure 7 and it can be seen that the COF under different normal loads behave somewhat differently from one another.

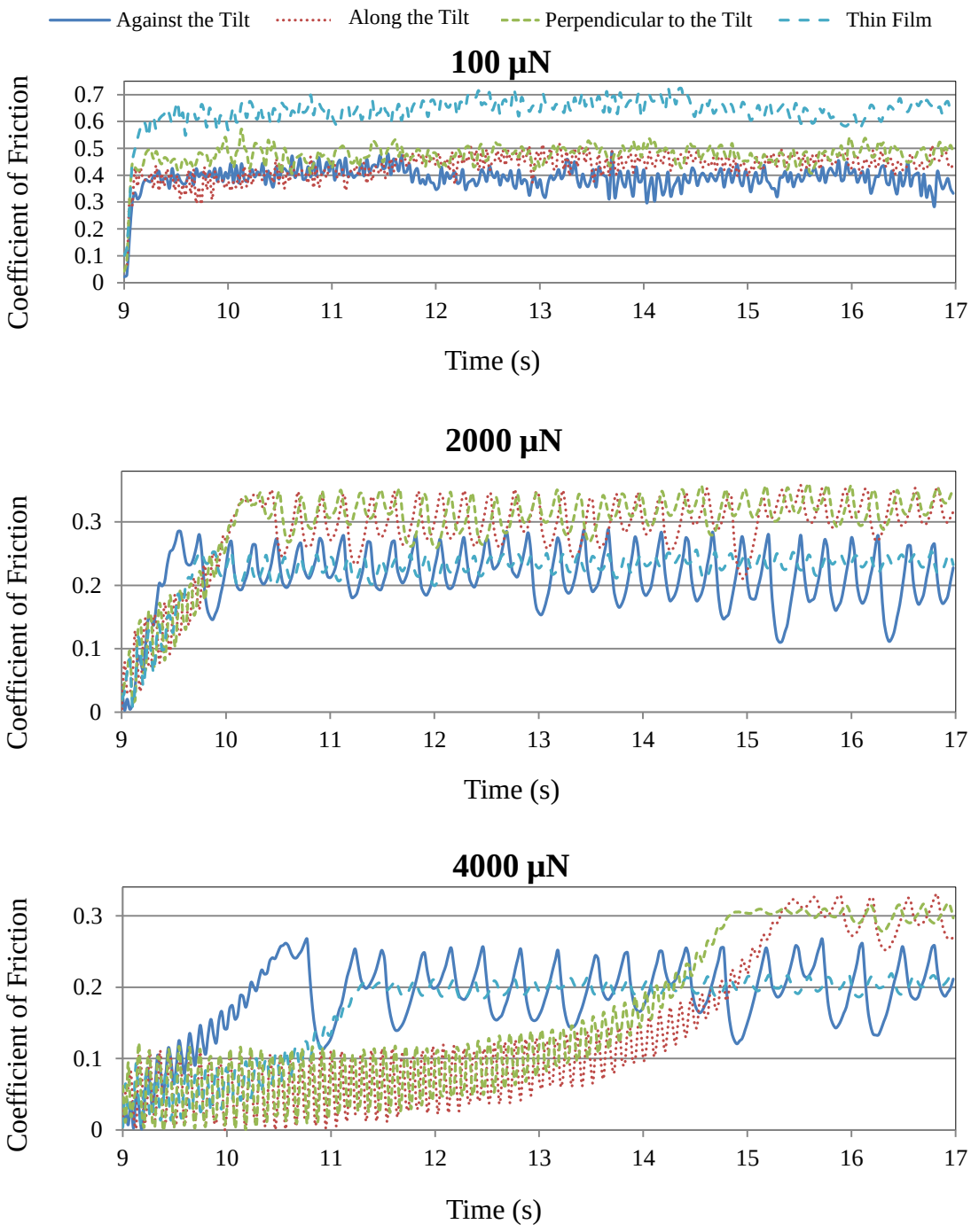

Figure 7: Typical COF curves for normal loads of 100 µN, 2000 µN, and 4000 µN.

First, notice that at the beginning of each scratch there is a period where the COF rises to level and then stabilizes. This rising period increases as the normal load increases for

several reasons. The main reason, however, is directly related to how the nanoindenter applies the normal load to the surface of the sample. The scratch begins by first having the tip hold its position and fully apply the chosen normal load. Once the loading is complete, the tip then begins to move the 8 microns required to complete the scratch. Consequently, the preloading procedure affects the area to be tested because the tip radius at 100 µm is incredibly large compared to the scratch length. The initial deformation that the preload causes increases with increases in the normal load, and this was seen to not significantly affect the test area until the normal load was increased to over 2000 µN. The effect of the preloading can also be seen visually under the ESEM.

In addition to the preloading effect, the high normal load scratches also exhibit an oscillatory behavior. The beginning portion of these scratches show an oscillation with a period of roughly 0.1 s on average, while the second stage of the scratch shows an oscillation period of between 0.2 s and 0.4 s. The second portion of the scratch has a much larger variation in period than the initial portion. Starting with the second portion of the scratch, these oscillations in the COF curve can be explained by the surface topography of the sample. The average spacing between the nanorod tips in the direction of the tilt is 320 nm with a variation of 100 nm. The tip moves at a speed of 1 µm/s and thus encounters a nanorod tip every 0.32 s on average. This falls within the period seen for each scratch and the variation of the period is most likely due to the varying nanorod-to-nanorod spacing and the fact that they are not arranged in a perfect linear pattern. The 0.1 s oscillation portion of the scratch corresponds to the area initially deformed during the tip's preloading process. The decrease in the period relates to the fact that the area

being tested is already deformed and smaller nanorods under the long ones create a surface with more frequent bumps. The low loads do not experience these oscillations because so few nanorods are being deformed.

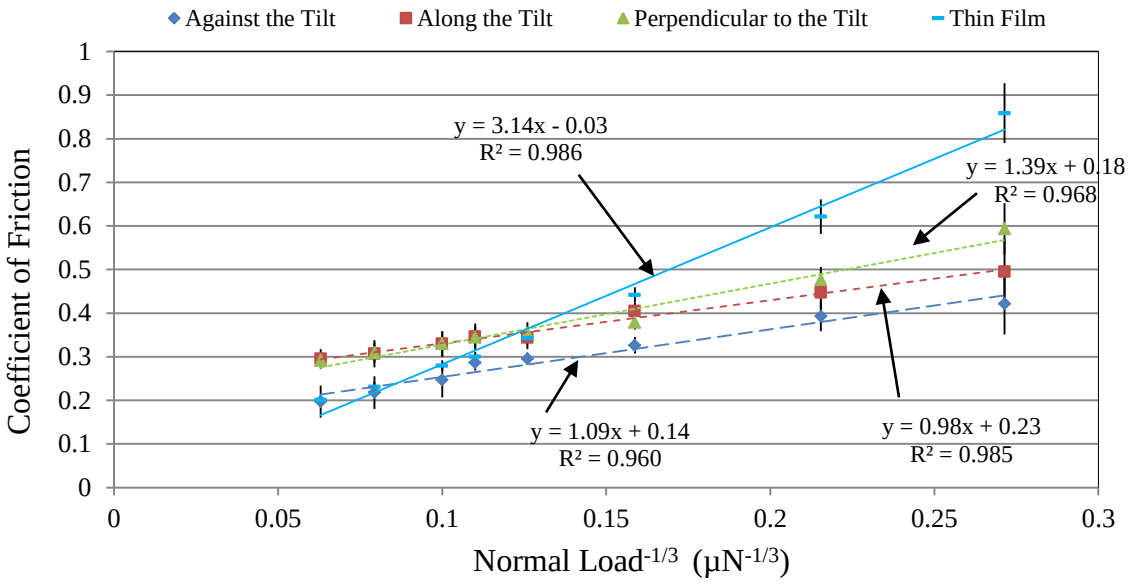

Figure 8: COF of the thin film and tilted nanorod samples for scratching directions along, against, and perpendicular to the tilt direction plotted against load$^{-1/3}$.

The relationship between the COF and the normal load to the power of -1/3 is displayed in Figure 8. There exists a linear relationship between them. This is due to the Hertzian model of contact mechanics (Johnson, 1985) which predicts the contact area of the tip is proportional to the normal load according to Equation 1.

$$a = \left(\frac{3PR}{4E^*}\right)^{1/3} \quad (1)$$

Here P is the normal load, E^* is the reduced Young's modulus, R the combined radius, and a the contact radius. The contact radius is shown in Figure 9 for indentation of the thin film. The radius of the sample is assumed to be infinite as it is a flat surface so the combined radius can be simplified from Equation 2 to Equation 3.

$$\frac{1}{R} = \frac{1}{R'} + \frac{1}{R''} \tag{2}$$

$$R = R' \tag{3}$$

In order for this simplification to be made though, the radius of the indenter tip must be significantly larger than the contact radius. For this study the indenter tip was 100 μm and the contact radius was determined to not exceed 5 μm when viewed under the ESEM. For the nanorod sample, the indentation method is the same with the exception that the sample radius can no longer be ignored because the tip is not penetrating a solid film, but rather the tips of each nanorod instead. Thereofore Equation 2 can not be simplified, but since the radius of the nanorods is known, the contact radius can still be determined. However, unlike the thin film sample, the indenter tip encounters a summation of extremely small contact points and not just a single large one. This has the affect of reducing the contact area on the nanorod sample compared to the thin film sample and is one of the reasons for the reduction of the COF on the textured surface.

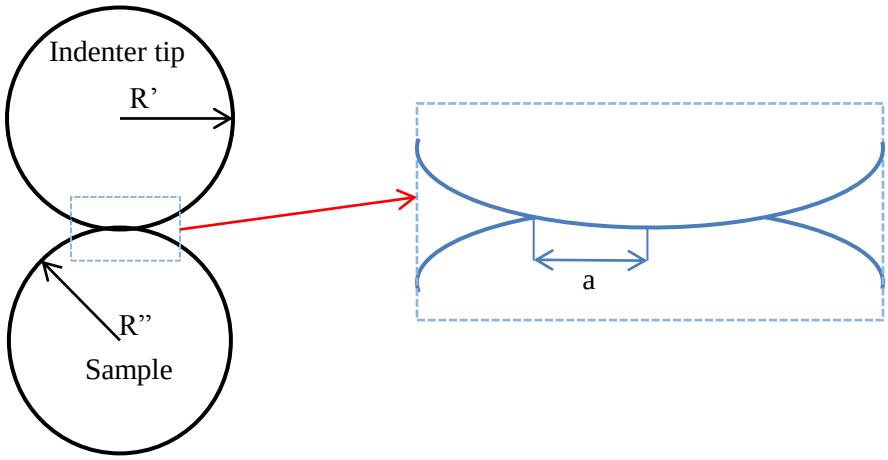

Figure 9: Diagram of the indenter tip and sample surface interaction.

The contact area of the tip is directly proportional to the square of the contact radius, thus because R and E* remain constant, the relationship in Equation 4 can be deduced.

$$A \propto P^{2/3} \tag{4}$$

A is the real contact area of the tip on the sample surface. According to adhesion theory of friction, friction is proportional to the real area of contact. Therefore using the definition for the coefficient of friction, the COF can be proportionally related to the normal load by Equation 5.

$$COF = \frac{F}{P} = \frac{A \times \tau}{P} \propto \frac{A}{P} \propto P^{-1/3} \tag{5}$$

Here τ is the shear strength of the material. Therefore, a linear relationship between the COF and normal load to the power of -1/3 suggests adhesion is the dominant mechanism of friction. Figure 8 shows that that while the relationship between COF and load is mostly linear, there is a flattening out of the curve as the load is increased (the left of Figure 8). This is because adhesion begins to play less of a dominating factor as the load is increased. Conversely, there is a slightly steeper slope at the very low loads. This effect is more pronounced in the nanorod samples than the thin film. The thin film also has a slope 36 percent steeper than the average slope of the textured sample, demonstrating the nanorod surface's ability to combat adhesion forces.

3.3 Deformation

The initial surfaces of the thin film and the tilted nanorod samples are shown in Figure 5. It is clear that both samples are very uniform. Furthermore, the tips of the nanorods are rounded but not flattened. An 8000 μN scratch for each test on the nanorod sample and the thin film are shown in Figure 10. The thin film sample had much less deformation than the nanorod sample and only the scratches caused by very high loads were discernible under the ESEM.

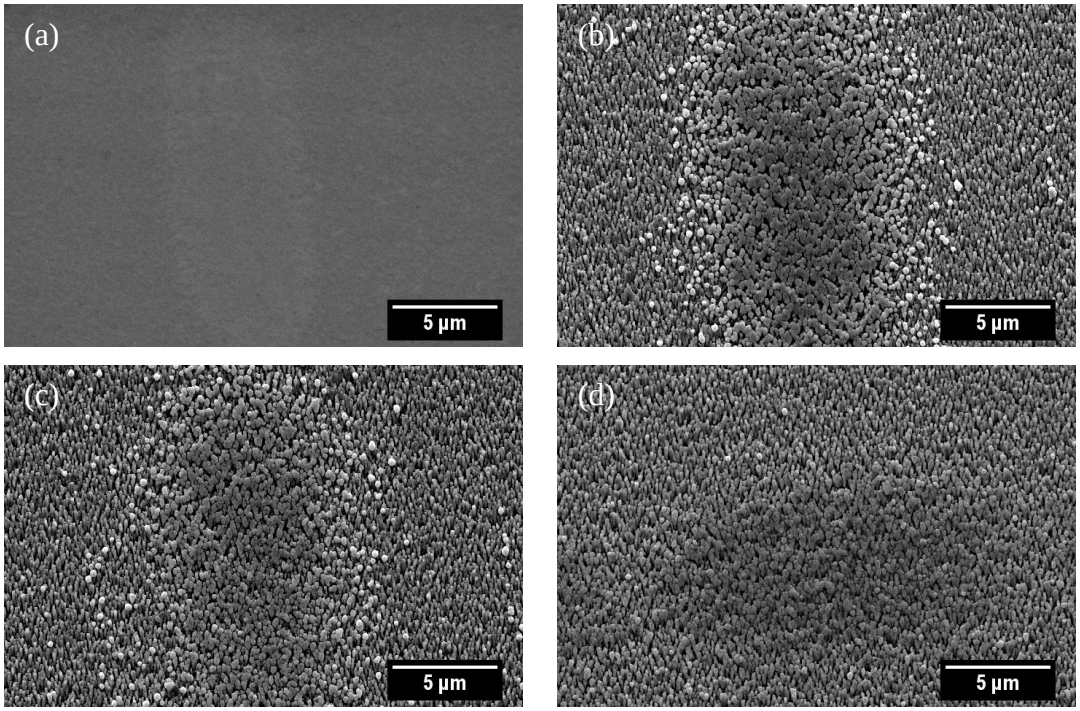

Figure 10: 8,000 µN scratches on (a) the thin film, (b) along the tilt, (c) against the tilt, and (d) perpendicular to the tilt.

Images were taken of the nanorod sample both with a gold sputtered coating and without. The sputtering, first applied to combat sample charging, had a very interesting unanticipated effect on the scratches by effectively highlighting the real contact area of each scratch. Figure 11 shows individual scratches performed on the nanorod sample for both the along and against directions at varying normal loads.

Starting with the lowest loads, the gold had a tendency to clump on top of the nanorods that had been slightly deformed by the scratch. This clustering is assumed to relate to the real area of contact due to the fact that it is not observed elsewhere on the surface and is located precisely where the scratch was located. Jumping now to the highest load, 8000 µN, two effects of the sputtering are observed on these scratches. First, the center of the

scratch is covered in a flat coating of gold and is much darker than the rest of the image. Second, the clumping effect seen in the low normal load scratches is also seen on the edges of the high normal load scratches.

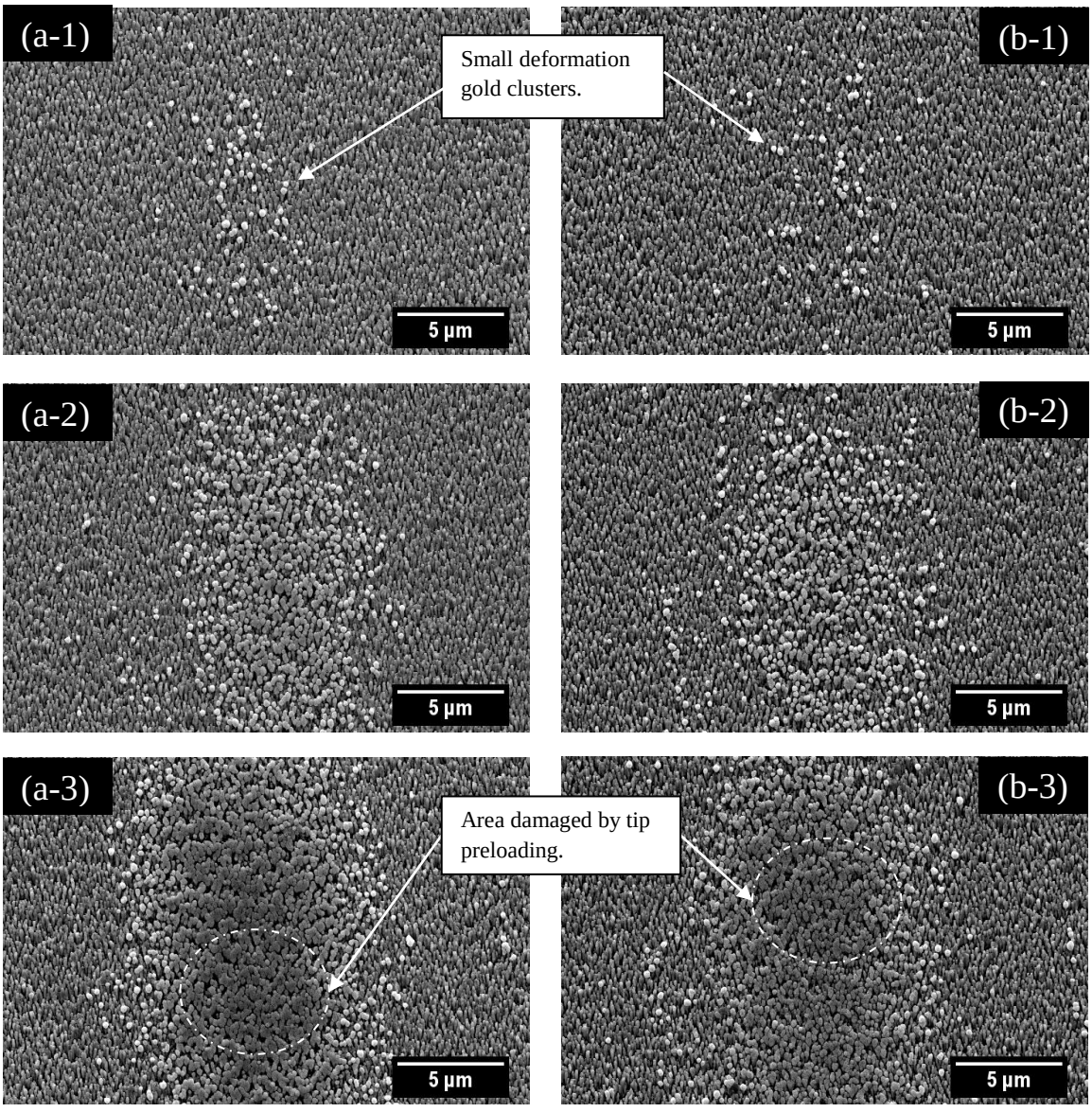

Figure 11: Individual scratches made (a) along and (b) against the tilt direction on the nanorod sample at loads of (1) 100 µN, (2) 2000 µN, and (3) 8000 µN at 5000x magnification.

The fact that the outside of the scratch is highlighted by the clumping effect can be attributed to the curved nature of the indenter's tip. The tip applies higher pressure on the center of the scratch, thus crushing and flattening the nanorods in the interior, but the exterior of the scratch does not experience the same pressure because the tip curves away from the sample and consequently deforms the edges to a lesser extent, which is similar to the low-load scratches.

In addition, Figure 12 compares ESEM images of a sputtered and nonsputtered 8000 μN scratch performed against the tilt. The nonsputtered scratch has the same characteristics of the sputtered scratch and verifies that the deformation seen after the sputtering is not merely a result of the sputtering itself.

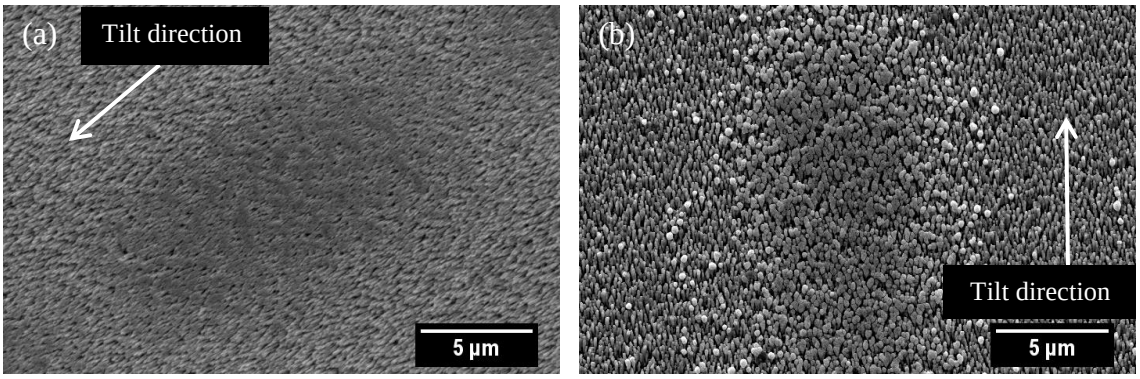

Figure 12: Comparison of an 8000 μN scratch performed against the tilt direction both (a) unsputtered and (b) sputtered.

The deformation of the nanorods, like the COF, also displays anisotropic behavior. Figure 11 displays the deformation caused by 100, 2000, and 8000 μN scratches performed in the along and against the tilt directions. The 100 μN scratches both appear to have very little damage done to their surfaces; in fact, the gold sputtering effect is the

sole reason that these scratch deformations were even visible. As would be expected, the deformation of the nanorods increases with every increase of the normal load. The anisotropic deformation behavior of nanorods is most apparent in the high load images. When viewed side by side, the scratch along the tilt direction has a noticeably more continuous film in the center of the scratch than the scratch against the tilt direction. Figure 13 shows a high-magnification comparison of the middle of the along and against scratch to highlight the greater amount of smearing in the along scratch.

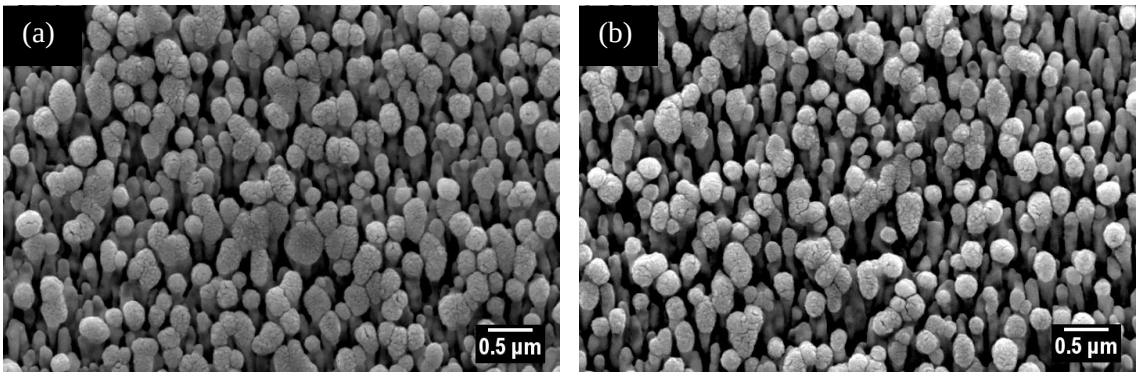

Figure 13: 20,000x magnification of a sputtered 2000 µN scratch performed (a) along and (b) against the tilt direction.

In addition, the nanorods have become more smeared together and form many large flattened clumps on the scratch along the tilt direction and the scratch against the tilt direction contains many more nanorods still as standalone structures. Indeed, this trend is seen throughout every normal load and is still easily discernible in the 2000 µN scratches shown. While it is harder to notice in the 100 µN scratch, there is a higher concentration of gold clusters present in scratches in the along direction than in the against direction.

4. Conclusion

The nanorod textured sample displayed many advantages over the non-textured thin film and proved to be an excellent way of reducing friction at low normal loads. The COF was lower on that sample than the thin film for all the scratching directions up to 250 μN. It also displayed anisotropic frictional behavior for all normal loads tested. In particular, the scratches performed against the tilt showed a much lower COF than both the thin film and scratching along the tilt direction. The COF of scratches performed against the tilt direction were over 30 percent lower than those performed along the tilt direction.

From this study, it can be concluded that the texturing of the sample was pivotal to the reduction of COF and that adjustments in the scratching direction can be used to control friction forces for various applications. The reduction in COF at low loads on the nanorod sample is most likely due to the texturing minimizing the strength of adhesion forces. Microprocessors and micro actuators could both greatly benefit with an applied nanotextured coating due to the reduction in adhesion forces. This would allow for devices to operate at lower powers and to be decreased in size. In addition, the deformation of the nanorods appeared to behave in an anisotropic manner as well. The scratch along the tilt direction proved to have consistently more deformation of the nanorods than the scratch against the tilt direction, especially under scratches of 2000 μN loads or more. The thin film however deformed much less than either of the nanorod samples due to the fact that the nanorods are standalone structures. The extensive damage done to the nanorods during high load tests is a result of silver's softness and malleability.

Due to the deformation of the nanorod film at high loads it is unclear as to whether they will continue to behave similarly if tested again. The ESEM images of high load scratches show a very continuous film in the middle of the scratch. The deformation under high normal loading is almost certainly responsible for the nanorods frictional behavior becoming similar to that of the thin film. Once the nanorod structures were collapsed they were not observed to recover and do indeed form a surface topography much like the thin film sample. The low load scratches were much less harmed and should continue to exhibit anisotropic behavior beyond one test. Indeed scratches performed at normal loads of less than 750 μN were not even visible under the ESEM without the layer of sputtered gold.

5. Future Work

5.1 Gold Sputtering

Further explanation of how and why the gold sputtering was able to highlight the real contact area of the indenter's tip needs to be investigated to determine whether or not it will work for other surface textures and different materials. There are several different factors that may be contributing to the sputtering's ability to highlight the contact area. The first factor is how the sputtering itself is applied to the sample surface. The length of the sputtering time controls the thickness of the gold layer on the sample's surface and is most likely one of the crucial factors in highlighting the contact area. It should be determined how thin the sputter layer can be to still mark the contact area and if there is a sputter thickness that becomes too thick and covers all of the sample features. In addition to the length of the sputtering time, the potential voltage applied during the sputtering process may be important to improving the highlighting effect. The potential voltage controls the size of the gold particles deposited on the sample surface. Varying the potential voltage at a constant sputtering time will determine if the gold particle size affects the sputtering's ability to highlight the contact area.

5.2 Friction and Deformation

The nanorod sample in this study exhibited the ability to reduce friction and behave in an anisotropic behavior and merits further investigations. More friction studies on nanorods samples arranged in different patterns and geometries on the surface will be conducted to

see how the arrangement affects the behavior of the film. Adjusting the nanorod pattern should affect the contact area of the indenter tip and result in different behavior of the COF and deformation. In addition, creating a patterned surface could increase the anisotropic behavior of the surface. Furthermore, the tilt angle of the nanorods and their length may be ways to alter both the COF and deformation of the nanorod sample as well. Deformation of the silver nanorods was very extensive under high normal loading during this study and changing materials may result in sturdier structures capable of withstanding greater pressures before deforming.

In order to determine the durability of the nanorod film, friction tests should be repeated on previously tested areas. Conducting these tests will be essential to determining how many cycles the nanorod film will continue to exhibit anistropic behavior at each load. It will also allow for further deformation studies to determine if repeated low load scratches will obtain the same deformation pattern as high load scratches. In addition, retesting of areas already scratched should affect the two-step behavior of the COF seen in the high load scratches of Figure 7. Indeed, no friction studies performed on tilted silver nanorods and very little characterization of the deformation caused by scratching the thin films have been completed before.

References

Ajayi, O. O., Erck, R. A., Lorenzo-Martin, C., & Fenske, G. R. (2009). Frictional anisotropy under boundary lubrication: Effect of surface texture. *Wear, 267*(5-8), 1214-1219.

Enomoto, Y., & Tabor, D. (1980). The frictional anisotropy of diamond. *Nature, 283*(5742), 51-2.

Hao, Z., Zhendong, D., & Songxiang, Y. (2008). Structure and friction characteristics of snake abdomen. *Journal of Nanjing University of Aeronautics & Astronautics, 40*(3), 360-3.

Hazel, J., Stone, M., Grace, M. S., & Tsukruk, V. V. (1999). Nanoscale design of snake skin for reptation locomotions via friction anisotropy. *Journal of Biomechanics, 32*(5), 477-84.

Hirakata, H., Nishihira, T., Yonezu, A., & Minoshima, K. (2011). Frictional anisotropy of oblique nanocolumn arrays grown by glancing angle deposition., 1-10.

Johnson, K. L. (1985). Contact Mechanics. Cambridge, Cambridgeshire: Cambridge UP. 84-104.

Komvopoulos, K. (2003). Adhesion and friction forces in microelectromechanical systems: Mechanisms, measurement, surface modification techniques, and adhesion theory. *J. Adhesion Sci. Technol., 17*(4), 477.

Lee, J., Fearing, R. S., & Komvopoulos, K. (2008). Directional adhesion of gecko-inspired angled microfiber arrays. *Applied Physics Letters, 93*(19), 191910 (3 pp.).

Morton, B. D., Wang, H., Fleming, R. A., & Zou, M. (2011). Nanoscale surface engineering with deformation-resistant core-shell nanostructures. *Tribology Letters, 42*(1), 51-58.

Nair, R. P., & Zou, M. (2008). Surface-nano-texturing by aluminum-induced crystallization of amorphous silicon. *Surface & Coatings Technology, 203*(5-7), 675-9.

Park, J. Y., Ogletree, D. F., Salmeron, M., Jenks, C. J., Thiel, P. A., Brenner, J., et al. (2008). Friction anisotropy: A unique and intrinsic property of decagonal quasicrystals. *Journal of Materials Research, 23*(5), 1488-1493.

So, E., Demirel, M. C., & Wahl, K. J. (2010). Mechanical anisotropy of nanostructured parylene films during sliding contact. *Journal of Physics D: Applied Physics, 43*(4)

Zmitrowicz, A. (2003). Glaciers and laws of friction and sliding. *Acta Mechanica, 166*(1-4), 185-206.

Zou, M., Cai, L., & Wang, H. (2006). Adhesion and friction studies of a nano-textured surface produced by spin coating of colloidal silica nanoparticle solution. *Tribology Letters, 21*(1), 25-30.

Zou, M., Cai, L., Wang, H., Yang, D., & Wyrobek, T. (2005). Adhesion and friction studies of a selectively micro/nano-textured surface produced by UV assisted crystallization of amorphous silicon. *Tribology Letters, 20*(1), 43-52.

Zou, M., Seale, W., & Wang, H. (2005). Comparison of tribological performances of nano- and micro-textured surfaces. *Proceedings of the Institution of Mechanical Engineers, Part N (Journal of Nanoengineering and Nanosystems), 219*(3), 103-10.

Zou, M., Wang, H., Larson, P. R., Hobbs, K. L., Johnsonb, M. B., & Awitor, O. K. (2006). Ni nanodot-patterned surfaces for adhesion and friction reduction. *Tribology Letters*, *24*(2), 137-42.